Journal of Modeling and Optimization 2021;13(2):58-79
https://doi.org/10.32732/jmo.2021.13.2.58

Closed-Loop Drive Detection and Diagnosis of Multiple Combined Faults in Induction Motor Through Model-Based and Neuro-Fuzzy Network Techniques

Imadeddine Harzelli, Abdelhamid Benakcha, Tarek Ameid, Arezki Menacer

LGEB Laboratory, Electrical Engineering Department, Faculty of Sciences and Technology, Biskra University, Biskra, Algeria
E-mail: imadeddineharzelli@yahoo.fr (Corresponding author)

Received: 21 April 2021; Accepted: 20 May 2021; Available online: 20 July 2021

Abstract: In this paper, a fault detection and diagnosis approach adopted for an input-output feedback linearization (IOFL) control of induction motor (IM) drive is proposed. This approach has been employed to detect and identify the simple and mixed broken rotor bars and static air-gap eccentricity faults right from the start its operation by utilizing advanced techniques. Therefore, two techniques are applied: the model-based strategy, which is an online method used to generate residual stator current signal in order to indicate the presence of possible failures by means of the sliding mode observer (SMO) in the closed-loop drive. However, this strategy is not able to recognise the fault types and it can be affected by the other disturbances. Therefore, the offline method using the multi-adaptive neuro-fuzzy inference system (MANAFIS) technique is proposed to identify the faults and distinguish them. However, the MANAFIS required a relevant database to achieve satisfactory results. Hence, the stator current analysis based on the HFFT combination of the Hilbert transform (HT) and Fast Fourier transform (FFT) is applied to extract the amplitude of harmonics due to defects occur and used them as an input data set for the MANFIS under different loads and fault severities. The simulation results show the efficiency of the proposed techniques and its ability to detect and diagnose any minor faults in a closed-loop drive of IM.
Keywords: Induction motor (IM); Input-output feedback linearization (IOFL) control; Fault detection and diagnosis; Stator residual current; Multi-adaptive neuro-fuzzy inference system (MANAFIS); Hilbert transform (HT).

1. Introduction

Nowadays, modern industrial systems are becoming more and more complex and sophisticated. At the same time reliability, availability and operating safety have become very important and real challenges for today's businesses. However, the squirrel cage induction motor, by its construction and its robustness, ensures a wide range of application in industrial systems [1]. The evolutions of power electronics, microelectronics and micro-computing have made it possible to overcome the problem of the non-linearity of the machine and to realize control algorithms that can make the IM a formidable competitor of speed variable [2]. There are many methods dedicated to control induction motors, however, the controlled part is subjected to strong nonlinearities and temporal variables, it is necessary to design control algorithms ensuring the robustness of the process against the uncertainties on the parameters and their variations. The input-output feedback linearization control has focussed on the attention owing to the simple design and on the perfect decoupling between rotor speed and flux, as well as fast dynamic response, even too easy implementation, robustness to parameter variations, and load disturbances [3–5].

The use of this machine in several industrial applications can be affected by potential defects; mechanical origin (rolling bearing wear, eccentricity of the shaft ...), electrical or magnetic (stator inter-turn short circuit, broken rotor bars ...), and supply (network or converter) [6–8]. Furthermore, the static air-gap eccentricity and broken rotor bars faults are the most important causes of faults in IMs, which lead to produce oscillation in the rotor speed and mechanical vibrations causing damage in IM. These faults effects become more apparent by increasing their severities, particularly, in the open-loop drives [9].

The tasks of detection and diagnosis of failures are naturally found their place in the monitoring system at closed-loop of IM. These tasks related to the knowledge acquired on the encountered problems, which make the fault detection and diagnosis approaches divided into two wide categories: approach with model [10] and approach without model [11].

Variable speed drives allow the machine to continue its operation even when the defects are exposed, which make the fault diagnosis delicate in the closed-loop drive, owing to the fact that the control-loop considered the defects may arise as a disturbance, and the IOFL control scheme corrects and compensate the faults effect. For that reason, the monitoring approach by approach with model, based on variable monitoring of the machine, is necessary. This approach required an observer that generally used to estimate the state variable of a system from the measurable inputs and outputs for the control system and it can be used also for fault detection [12]. Many structures of observers have been proposed in literature such as model reference adaptive system MRAS [13], sliding mode observer [14,15], Luenberger observer [16], and high gain observer [17]. The fault detection technique based on a formal model of the machine to be monitored, it does not depend on the nature of the signal, which provides a good prognosis of the faults in transient and steady states of IM. Moreover, the formal model will serve as a reference for defining the normal operation, and any deviation from the operating point will be a sign of the failure [18].

The model-based strategy is an analytical model based on the monitoring of the parameters and the magnitudes of the machine, by means of observation algorithms. This strategy detects the faults by comparing the model and the actual process referring to the evolution of the residual signals [19]. A SMO is used, due to the conception simplicity and the computational efficiency, in order to obtain a vector of stator residual current in the closed-loop motor drive to achieve rapid fault detection. Many researchers have focused their attention on the use of a model-based strategy for fault detection. In this area, [20] has developed a model-based strategy to detect the stator short-circuit fault in the IM. This strategy based on the generation of a specific current residual vector using a state observer. The proposed strategy presents very low sensitivity to load variations and power-supply perturbations and show the ability for detecting incipient faults, including a low number of short-circuited turns. In [21], a fault detection method is proposed for IM based on a high-order sliding mode observer. This technique is used to detect the stator windings damages and shows that the current and speed residual signals sensitive to the fault occurs. On the other hand, the model-based strategy can use the whiteness of innovation sequence developed by the standard extended Kalman filter. This technique just requires current sensors, which are available in most IM drive systems to provide good controllability. This proposed method provides better estimates for stator inter-turn fault detection as mentioned in [22]. Furthermore, a new model-based fault detection and isolation (FDI) strategy is proposed in [23] for field-oriented control, IM drives. The residual evaluation generated by the single open-circuit faults is carried out in the stator reference frame (dq-coordinates). The observer FDI scheme can be combined with a fault re-configuration strategy in order to improve the reliability of the motor drive, which leads to the effective detection of single open-circuit faults. The work of [24], used the rotor speed residual for sensor fault detection in IM drives by means of the single adaptive observer. The current model-based approaches, presented by an algebraic equations-based analysis, ensure the fast detection of speed sensor fault scenarios.

In fact, these residuals are sensitivity for modelling uncertainties, parameter variation, load disturbance, and the unknown inputs such as external noise, which lead to a false alarm, and it is difficult to distinguish the simultaneous faults. In order to overcome this problem and solve the ambiguity in IM, the modeless methods (approach without model) are applied.

Modeless methods are divided into two parts, the first part corresponding to low-level processing tools. It is based on the extraction of information through the measured signals processing tools which are currents, voltages, speed, vibrations, temperature, and noise emissions. However, the stator current signals can provide a significant information on faults using the spectrum through the fast Fourier transform, short time Fourier transform (STFT), and wavelet transform (WT) [2,25]. Generally, the FFT is used to determine the spectral signatures by investigating the frequencies components around the fundamental frequency for each fault in IM [26]. Nevertheless, FFT suffers from its sensitivity to load variations conditions [27]. Furthermore, at low slip, FFT technique can not offer efficient detection performance, due to the rapprochement and overlap of the broken rotor bars $(1\pm2ns)f$ and static air-gap eccentricity $(mf_r\pm f)$ $(m, n=1,2,3...)$ faults frequencies characteristic in the stator current with the fundamental frequency component as their amplitudes are small to compare. Advanced signal processing techniques are needed to be considered to avoid the FFT drawback. For that reason, one or more signal processing technique may be combined for more efficient fault diagnosis as presented in [25], the authors used the DWT and HT to achieve high accuracy to detect broken rotor bars fault in IM. In this paper, the HFFT technique is proposed to extract the envelope from the stator current by HT and processed it via FFT. This combination presents a significant tool to distinguish the simple and mixed faults occur with high resolution even at low slip, without overlap between the faults frequencies.

Second part so-called high-level techniques, which use tools more oriented towards the communication between experts. However, the techniques of artificial intelligence serve as basic tools for decision support. A lot of researches developed by academics and industry are reported in the literature to identify the faults in the induction machines [28,29]. Out of many artificial intelligence techniques used for the motor fault diagnosis, particularly in this present work, the adaptive neuro-fuzzy inference system (ANFIS), which is a combination of fuzzy logic and neural network techniques [30]. Recently, ANFIS is combined with other methods and is employed as an enhanced

tool for conducting classification. The work by [31] the neuro-fuzzy technique has been used to detect the broken rotor bars using FTT to extract the features from the magnetic flux density, which were considered as an input for the proposed technique. In [32], a new methodology for stator inter-turn fault diagnosis of three-phase IM using ANFIS is presented, which is developed based on Sequence Component Phase Index and Sequence Component Amplitude Index for detection of fault location and fault severity. Furthermore, the fault diagnosis of squirrel-cage induction motor broken bars based on ANFIS identification method with subtractive clustering is presented by [33], this concept is implemented by primarily taking into account the information data extracted from the classical motor current signature analysis (MSCA), then ANFIS approach used this data set as an input for early rotor bar fault detection phase. In [34], the field of monitoring and diagnosing IM faults, particularly the stator short-circuit, the broken rotor bar faults and the mixed fault is carried out, based on the neuro-fuzzy network technique. Its knowledge base makes use of indicators derived from DWT analysis and spectral analysis of the stator current, which allows, in addition to the detection, the evaluation of the number of broken bars and the position of the turns in short-circuit. The hybrid model, known as FMM-CART (the Fuzzy Min-Max neural network and the Classification and Regression Tree), is used to detect and classify fault conditions of IM in both offline and online motor operations as reported in [35]. The broken rotor bars, stator winding, and unbalanced supply faults, are investigated to evaluate the effectiveness of FMM-CART. The signal harmonics are extracted from the power spectral density (PSD), and used them as the input data for faults classification with FMM-CART, the results indicate that method is able to detect and diagnosis the faults in the early stage. Authors in Ref. [36], investigated the current monitoring for effective broken rotor bar fault diagnosis in open loop of IM, by using a novel oblique RF (random forest) algorithms classifier. Therefore, the RF algorithm prove to be relevant for the motor diagnosis. Phuong et al. [37] presented a diagnosis methodology for incipient rolling element bearing failures; by extract useful features from incoming acoustic emission signals by using a wavelet packet transform based kurtogram. The linear discriminant analysis (LDA) technique is used to select the most discriminant bearing fault features from the original feature set. Then, a Naïve Bayes (NB) classifier used the selected fault features in order to classify the bearing fault conditions and it shows good accuracies for classification. Furthermore, the Authors in Ref. [38,39] used the vibrations analysis methods to diagnose the bearing faults by using, respectively; spectral kurtosis (SK) based feature extraction coupled with k-nearest neighbor (KNN) distance analysis, and an adaptive deep convolutional neural network (ADCNN), which is used the cyclic spectrum maps (CSM) of raw vibration signal as bearing health states. That is lead to automate feature extraction and classification process. Slaheddine et al. [40] improve the standard support vectors machines (SVM) by using support vector data description (SVDD) based on MCSA and stationary wavelet packet transform (SWPT) for feature extraction to diagnose broken rotor bar fault. Bensaoucha et al. [41] proposed a diagnostic technique based on NN for detecting and locating the inter turns short-circuit in one of three stator winding phases of IM, where the three-phase shift between the stator voltages and its currents are considered as inputs of the NN in order to develop an automatic fault detection and classification system. The authors in [42], used methods for bearing fault detection and diagnosis by means of the artificial neural network (ANN) and ANFIS. The multi-staged decision algorithm is developed based on ANN and ANFIS models. Both time and frequency domain parameters extracted from the vibration and current signals are used to train the ANN and ANFIS models, which are then used to detect and diagnose the severity of the bearing fault. The results revealed that ANFIS-based scheme is superior to the ANN-based one especially in diagnosing fault severity. As well, the ANFIS conception presents a limitation to identify the mixed faults due to a single output. Further, the most techniques of artificial intelligence are used in the literature for an open-loop machine process in several cases. Nevertheless, in closed-loop drives, the control-loop compensates the fault effect [43], which cause difficulty in diagnosis defects. Based on the aforementioned state of the art, the Multi-ANFIS (MANFIS) technique proposed in this work to overcome the problem of accuracy and single ANFIS output, which is used to identify and distinguish the mixed and the simple faults of the broken rotor bars and static air-gap eccentricity even at low slip in IM closed-loop drives. This technique used the features extracted from the HFFT technique under different loads and fault severities as an input data set for the training algorithm.

In this context, the important aim of this paper is to show another perspective with regard to the detection and diagnosis of the fault in a closed loop of induction motors. The reduced model of the IM dedicated to simulate two of faults: broken rotor bars and static air-gap eccentricity. The implementation of IOFL control by means of the SMO is proposed in order to estimate the stator current in healthy and faulty states of the induction machine. The model-based approach is operated for fast detection of incipient faults using SMO through the residual stator current. As well, the HFFT technique extracts the amplitudes of frequency components due to the defects occurs in IM from the stator current envelope (SCE) under different loads and fault severities. These features are considered as reliable indicators and used them as input data set for MANAFIS. The obtained results show the value of the proposed techniques for fault detection and diagnosis in a closed-loop drive of IM.

2. Spectrum of stator current envelope and model-based approach

All *text* should be Times New Roman and in a one-column format. Do not change the columns wide as they have been set in the template.

Hilbert transform is a signal analysis method used to extract the stator current envelope as illustrated in Fig. 1. However, the HT is a time domain convolution of a signal *x(t)* with the function *1/t*, such as the phase current that is used to emphasize its local properties, as follows [25,44] :

$$H\left[x(t)\right]=\frac{1}{\pi}\int_{-\infty}^{+\infty}\frac{x(\tau)}{t-\tau}d\tau=x(t)*\frac{1}{\pi t} \tag{1}$$

Where *t* is time, *x(t)* is a time-domain signal, * is the convolution indicates, and *H[x(t)]* is the Hilbert transform of *x(t)*.

Spectrum analysis of stator current envelope via FFT technique allows the recognising the sidebands of fault frequency components, practically the broken rotor bars (*2nsf*) and static air-gap eccentricity (mf_r).

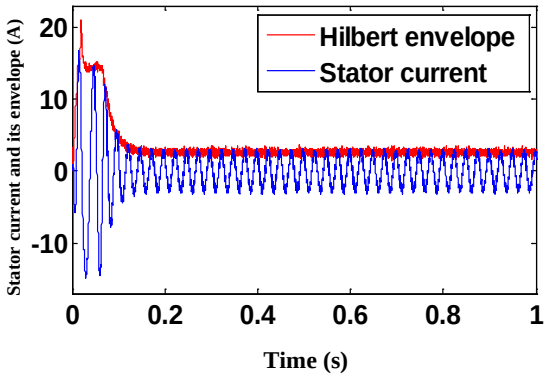

Figure 1. Stator current and its envelope for healthy motor.

A model-based approach is a concept of analytical redundancy by means of observers in terms of estimated and measured outputs ($I_{abc}-\hat{I}_{abc}$), The main equation of residual stator current $r_I(t)$ is written as [19].

$$r_I(t)=Z_p(I_{abc}-\hat{I}_{abc}) \tag{2}$$

where, Z_p is a weighting matrix.

The windowed norm can be performed to each residual as follows:

$$\|r_I\|=\sqrt{\frac{1}{T}\int_t^{t+T}(r_I(t))^2\,dt} \tag{3}$$

Fig. 2 shows that the diagnostic logic consists of making decisions from the evaluation of residual stator current $r_I(t)$.

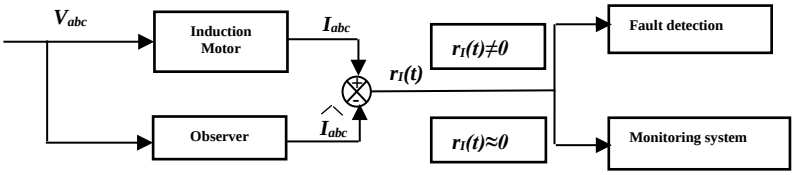

Figure 2. Fault detection logic of model-based strategy.

3. Reduced model of IM taking into account the faults

The study of any physical system often requires a modelling in order to simulate its behaviour against different constraints; to highlights the influence of defects on a measurable magnitude of the machine, and ensures to apprehend the mechanisms governing its operation [45,46]. The development of a mathematical reduced model is obtained from the multi-winding model of IM as shown in Fig. 3; taking into account the rotor faults such as broken rotor bars and static air-gap eccentricity. An extended Park's transformation will be applied to the rotor system to transform N_r bars system into *(d, q)* system. Afterwards, the system can be written as follows [43]:

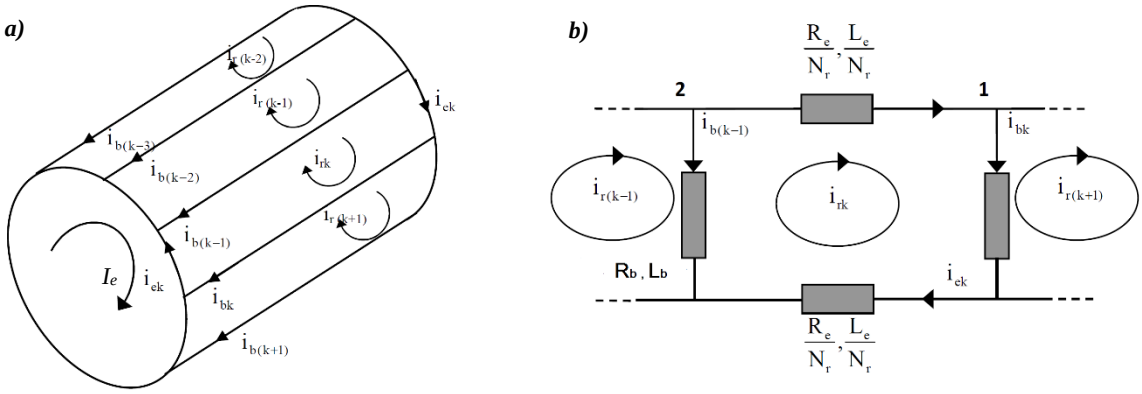

Figure 3. Rotor cage of induction machine. **a)** Structure. **b)** Equivalent circuit.

$$[L]\frac{d[I]}{dt}=[U]-[R][I] \tag{4}$$

where

$$[U]=\begin{bmatrix}U_{ds} & U_{qs}\end{bmatrix}^T,[I]=\begin{bmatrix}I_{ds} & I_{qs} & I_{dr} & I_{qr} & I_e\end{bmatrix}$$

with

$$[L]=\begin{bmatrix} L_{sc} & 0 & -\frac{N_r}{2}M_{sr} & 0 & 0 \\ 0 & L_{sc} & 0 & -\frac{N_r}{2}M_{sr} & 0 \\ -\frac{3}{2}M_{sr} & 0 & L_{rc} & 0 & 0 \\ 0 & -\frac{3}{2}M_{sr} & 0 & L_{rc} & 0 \\ 0 & 0 & 0 & 0 & L_e \end{bmatrix}$$

and

$$[R]=\begin{bmatrix} R_s & -\omega_r L_{sc} & 0 & \frac{N_r}{2}\omega_r M_{sr} & 0 \\ \omega_r L_{sc} & R_s & -\frac{N_r}{2}\omega_r M_{sr} & 0 & 0 \\ 0 & 0 & \begin{bmatrix}R_{rdd}=R_r\end{bmatrix} & \begin{bmatrix}R_{rdq}=0\end{bmatrix} & 0 \\ 0 & 0 & \begin{bmatrix}R_{rqd}=0\end{bmatrix} & \begin{bmatrix}R_{rqq}=R_r\end{bmatrix} & 0 \\ 0 & 0 & 0 & 0 & R_e \end{bmatrix}$$

The total cyclic inductance of a stator phase is equal to the sum of the magnetizing and leakage inductances:

$$L_{cs}=L_{sp}+L_{sf} \tag{5}$$

where,

$$L_{sp}=4\mu_0\frac{N_s^2 R.l}{e.p^2\pi}$$

The maximum value of the stator/rotor mutual inductance is:

$$M_{sr} = (4/\pi)(\mu_0/e.p^2)N_s.R.l\sin(a/2) \tag{6}$$

The electrical angle of two adjacent rotor meshes:

$$\alpha = p\frac{2\pi}{N_r}$$

The cyclic rotor inductance is given by the following:

$$L_{rc} = L_{rp} - M_{rr} + 2\frac{L_e}{N_r} + 2L_e(1-\cos\alpha) \tag{7}$$

The principal inductance of a rotor mesh can be calculated by

$$L_{rp} = \left(\frac{N_r - 1}{N_r^2}\right)\frac{\mu_0}{e}2\pi.R.l$$

The mutual inductance between non-adjacent rotor meshes is defined by

$$M_{rr} = \frac{1}{N_r^2}\frac{\mu_0}{e}2\pi.R.l$$

The electromagnetic torque developed by the motor is expressed in terms of rotor currents and stator currents as:

$$T_e = -\frac{3}{4}pN_rM_{sr}\left(I_{dr}I_{qr} - I_{qr}I_{ds}\right) \tag{8}$$

By considering the electromagnetic torque equation, the rotor speed is given as follows:

$$\frac{d\omega_r}{dt} = \frac{1}{J}(T_e - T_L - F\omega_r) \tag{9}$$

3.1 Broken rotor bar fault

The four terms resistances of broken rotor bar fault (Fig. 4) are given by:

$$\begin{cases} R_{rdd,rqq} = R_r + \dfrac{2}{N_r}(1-\cos\alpha)\sum\limits_k R_{bfk}.\left(1 \pm \cos(2k-1).\alpha\right) \\ R_{rdq,rqd} = -\dfrac{2}{N_r}(1-\cos\alpha)\sum\limits_k R_{bfk}.\sin(2k-1).\alpha \end{cases} \tag{10}$$

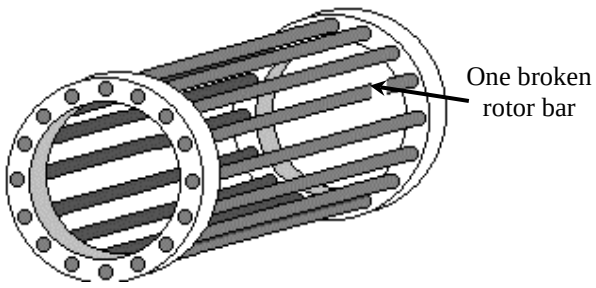

Figure 4. Broken rotor bar of induction machine.

In this expression, the summation is applied to all bars with fault. R_{bfk} is the resistance of the bar index k from its initial value before the fault.

3.2 Static air-gap eccentricity fault

The static air-gap eccentricity fault is illustrated in Fig. 5, where the magnetomotive force of the stator windings is assumed sinusoidal. The winding function theory is applied for computational of mutual inductance between the stator coils and rotor loops in an induction motor taking into account the air-gap eccentricity fault can be expressed as [47,48]:

$$M_{sr}(\theta_r) = \mu_0 Rl \int_0^{2\pi} n_{rk}(\theta_r, \varphi) N_{sq}(\theta_r, \varphi) g_e(\theta_r, \varphi)^{-1} d\varphi \tag{11}$$

The term $n_{rk}(\theta_r, \varphi)$ is the winding distribution of K_{th} rotor loop, and $N_{sq}(\theta_r, \varphi)$ is called the modified winding function of phase $''q''$. The inverse air-gap length at any position θ_r can be illustrated as:

$$g_e(\varphi)^{-1} = \frac{1}{e}(1 + \varepsilon_s \cos\varphi), \text{ where } \varepsilon_s = \frac{o_s o_r}{e}.$$

All the motor inductances can be calculated using Eq. (11) and [47,48].

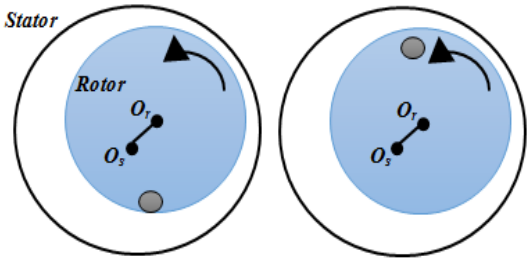

Figure 5. Static air-gap eccentricity Illustration.

4. Input-output feedback linearization control and sliding mode observer using the reduced model of IM

4.1 Input-output feedback linearization control

The input-output feedback linearization strategy makes it possible to find a state feedback loop in order to transform a nonlinear system into a fully or partially linear one [5]. The technique requires measurements of the state vector x in order to transform a multi-input nonlinear control system into a linear and controllable one. The state space model of an induction motor in the (α, β) frame coordinate is given by [4]:

$$\begin{cases} \dot{x} = f(x) + g(x).u(t) \\ y = h(x) \end{cases} \tag{12}$$

Where the state and control vectors are expressed as:

$$\begin{cases} x = \begin{bmatrix} I_{s\alpha} & I_{s\beta} & \Phi_{r\alpha} & \Phi_{r\beta} & \omega_r \end{bmatrix}^T = \begin{bmatrix} x_1 & x_2 & x_3 & x_4 & x_5 \end{bmatrix}^T \\ u = \begin{bmatrix} U_{s\alpha} & U_{s\beta} \end{bmatrix}^T \end{cases}$$

with

$$\begin{bmatrix} \dot{x}_1 \\ \dot{x}_2 \\ \dot{x}_3 \\ \dot{x}_4 \\ \dot{x}_5 \end{bmatrix} = \begin{bmatrix} a_{r11}x_1 + a_{r12}x_3 + a_{i12}x_4x_5 + b_1U_{s\alpha} \\ a_{r11}x_2 + a_{r12}x_4 - a_{i12}x_3x_5 + b_1U_{s\beta} \\ \frac{M}{Tr}x_1 - \frac{1}{Tr}x_3 - px_4x_5 \\ \frac{M}{Tr}x_2 - \frac{1}{Tr}x_4 + px_3x_5 \\ \eta(x_2x_3 - x_1x_4) - \frac{T_L}{J} - \frac{F}{J}\omega_r \end{bmatrix} \tag{13}$$

Let

$$y = \begin{bmatrix} y_1 \\ y_2 \end{bmatrix} = \begin{bmatrix} h_1(x) \\ h_2(x) \end{bmatrix} = \begin{bmatrix} \omega_r \\ \Phi_r^2 = \Phi_{r\alpha}^2 + \Phi_{r\beta}^2 \end{bmatrix} \tag{14}$$

where

$$\eta = -\frac{3}{4} pN_r M_{sr}\ , M = -\frac{3}{2} M_{sr}\ ,\ T_r = \frac{L_{rc}}{R_r}\ ,\ \begin{cases} a_{r11} = \frac{1}{T_r}\left(\frac{\sigma - 1}{\sigma}\right) - \frac{R_S}{\sigma L_{sc}}\ , a_{r12} = \left(\frac{1}{T_r}\right)\left(\frac{\sigma - 1}{\sigma} \cdot \frac{2}{3M_{sr}}\right) \\ a_{r11} = \frac{1}{T_r}\left(\frac{\sigma - 1}{\sigma}\right) - \frac{R_S}{\sigma L_{sc}}\ , a_{r12} = \left(\frac{1}{T_r}\right)\left(\frac{\sigma - 1}{\sigma} \cdot \frac{2}{3M_{sr}}\right) \end{cases}$$

The Lie derivative notation is used for state function $h(x)$: $R_n \longrightarrow R$ along a vector field $f(x)$ can be written as follows [4]:

$$L_f h = \sum_{i=1}^{n_1} \frac{\partial h}{\partial x_i} f_i(x) \tag{15}$$

Iteratively, we get $L_f^i h = L_f\left(L^{(i-1)}{}_f h\right)$.

The change of coordinates is defined as:

$$\begin{cases} z_1 = h_1(x) = x_5 \\ z_2 = L_f h_1(x) = \eta(x_2 x_3 - x_1 x_4) - \frac{T_L}{J} - \frac{F}{J} x_5 \\ z_3 = h_2(x) = x_3^2 + x_4^2 \\ z_4 = L_f h_2(x) = -\frac{2}{T_r}\left(x_3^2 + x_4^2\right) + 2\frac{M}{T_r}\left(x_3 x_1 - x_4 x_2\right) \end{cases} \tag{16}$$

Thus, the derivatives of the outputs are given in the new coordinate system by:

$$\begin{cases} \dot{z}_1 = \dot{h}_1(x) = z_2 \\ \dot{z}_2 = \ddot{h}_1(x) = L_f^2 h_1(x) + L_{g_1} L_f h_1(x) U_{s\alpha} + L_{g_2} L_f h_1(x) U_{s\beta} \\ \dot{z}_3 = \dot{h}_2(x) = z_4 \\ \dot{z}_4 = \ddot{h}_2(x) = L_f^2 h_2(x) + L_{g_1} L_f h_2(x) U_{s\alpha} + L_{g_2} L_f h_2(x) U_{s\beta} \end{cases} \tag{17}$$

This system can be written as:

$$\begin{bmatrix} \ddot{z}_1 \\ \ddot{z}_3 \end{bmatrix} = \begin{bmatrix} \dot{z}_2 \\ \dot{z}_4 \end{bmatrix} = \begin{bmatrix} L_f^2 h_1(x) \\ L_f^2 h_2(x) \end{bmatrix} + D(x) \begin{bmatrix} U_{s\alpha} \\ U_{s\beta} \end{bmatrix} \tag{18}$$

The decoupling matrix $D(x)$ is defined as:

$$D(x) = \begin{bmatrix} L_{g_1} L_f h_1(x) & L_{g_2} L_f h_1(x) \\ L_{g_1} L_f h_2(x) & L_{g_2} L_f h_2(x) \end{bmatrix} \tag{19}$$

The decoupling matrix D(x) has a singularity which occurs at the start-up of the IM (Φ_r^2=0). To handle this situation, one can use an open loop controller at the start-up of the machine, thereafter switch to the nonlinear controller once the flux goes up to zero. The nonlinear state feedback control can be modelled as:

$$\begin{bmatrix} U_{s\alpha} \\ U_{s\beta} \end{bmatrix} = D^{-1}(x) \begin{bmatrix} U_1 - L_f^2 h_1(x) \\ U_2 - L_f^2 h_2(x) \end{bmatrix} \tag{20}$$

This controller linearizes and decouples the system, resulting in:

$$\begin{cases} \ddot{h}_1 = U_1 \\ \ddot{h}_2 = U_2 \end{cases} \tag{21}$$

From Eq. (21), the input-output of a closed loop system is decoupled and linearized. To ensure perfect tracking of speed and flux references, U_1 and U_2 are chosen as follows:

$$\begin{cases} U_1 = -k_1\left(\omega_r - \omega_{ref}\right) - k_2\left(\dot{\omega}_r - \dot{\omega}_{ref}\right) + \ddot{\omega}_{ref} \\ U_2 = -k_3\left(\Phi_r - \Phi_{ref}\right) - k_4\left(\dot{\Phi}_r - \dot{\Phi}_{ref}\right) + \ddot{\Phi}_{ref} \end{cases} \tag{22}$$

Where k_1, k_2, k_3, and k_4 are positive non-zero constants to be determined to make sure that closed loop system from Eq. (21), stable and to have a fast response to variable tracking.

4.2 Sliding mode observer

The reduced model of IM is used to design the SMO to establish a good compromise between the stability and the simplicity of the observer [15]. The state equation of the observer can be written in the following way:

$$\frac{d}{dt}\begin{bmatrix} \hat{I}_{s\alpha\beta} \\ \hat{\Phi}_{r\alpha\beta} \end{bmatrix} = \begin{bmatrix} -\frac{R_r}{\sigma L_{sc}} I_2 & \frac{M}{\sigma L_{sc} L_{rc} T_r} - J_2 \frac{M}{\sigma L_{sc} L_{rc}} \omega_r \\ \frac{M}{T_r} I_2 & -\frac{M}{T_r} I_2 + J_2 \omega_r \end{bmatrix} \begin{bmatrix} I_{s\alpha\beta} \\ \Phi_{r\alpha\beta} \end{bmatrix} U_{s\alpha\beta} + \begin{bmatrix} K_s \\ K_r \end{bmatrix} \begin{bmatrix} sign(S_1) \\ sign(S_2) \end{bmatrix} \tag{23}$$

where

$$I_{s\alpha\beta} = \begin{pmatrix} I_{s\alpha} \\ I_{s\beta} \end{pmatrix}, \Phi_{r\alpha\beta} = \begin{pmatrix} \Phi_{r\alpha} \\ \Phi_{r\beta} \end{pmatrix}, U_{s\alpha\beta} = \begin{pmatrix} U_{s\alpha} \\ U_{s\beta} \end{pmatrix}, J_2 = \begin{pmatrix} 0 & -1 \\ 1 & 0 \end{pmatrix}.$$

I_2 is the identity matrix *2x2*.

$$K_i = \begin{bmatrix} K_S \\ K_r \end{bmatrix}$$

is the matrix of the observer correction gains.

$$S_i = \begin{bmatrix} S_1 \\ S_2 \end{bmatrix} = \begin{bmatrix} I_{s\alpha} - \hat{I}_{s\alpha} \\ I_{s\beta} - \hat{I}_{s\beta} \end{bmatrix}$$

is the sliding surface of the current error.

Where

$$\begin{cases} sign(S_i) = +1 \text{ if } S_i > 0 \\ sign(S_i) = -1 \text{ if } S_i < 0 \end{cases}$$

5. Simulation results for Input-output feedback linearization control IM

The input-output feedback linearization control of IM used in the healthy and faulty state: 1.1 kW, 220V, 50Hz, 2-pole, a rotor with 16 bars were carried out using the Matlab/Simulink simulation package. The system parameters of the induction motor tested in this study are given in the Appendix.

Fig. 6 presents the input-output feedback linearization control diagram block using the sliding mode observer for stator current and flux estimation.

The variable frequency drive (VFD) is considered as energy saving drives, but on the other hand it generates noise in the line currents. However, the input-output linearization control used pulse width modulation (PWM) by

means of VFD for controlling of IM. This robust combination (IOFL control+ PWM) has the advantage to control a device with high precision and minimize the natural noise due to VFD, which allows a good diagnosis of IM. The VFD used in this simulation composed of a rectifier and IGBT inverter uploaded from Matlab/Simulink in order to take into account the noise. The PWM switching sequences are calculated with a commutation frequency equal to 4 kHz. A supply voltage of (400 V) is filtered through the rectifier in order to fix the U_{DC} bus of the inverter. The noise generated by a VFD reduces its signal to noise ratio (SNR). A white Gaussian noise of 10 dB of SNR (low SNR) added to the output voltages (U_a, U_b, U_c), in order to model the other noise.

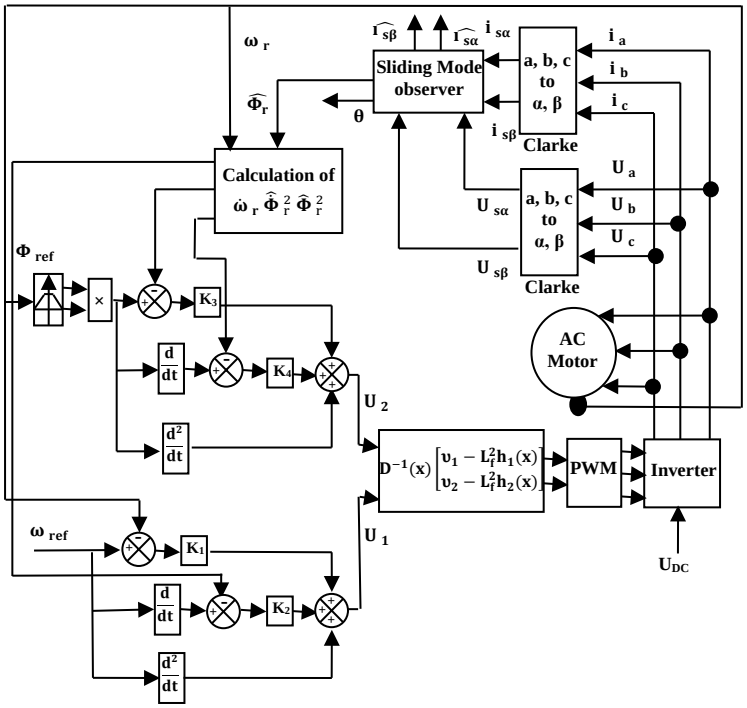

Figure 6. Global block diagram of input-output feedback linearization control.

5.1 Healthy state of the machine

To illustrate the performances of the controller in a healthy state of IM, a simulation with reference speed equal to 2600 rpm is realized in Fig. 7, a nominal load torque equal to 3.5 Nm is applied at t=0.5s. The sampling rate considered in this simulation 10kS/s using the Matlab/Simulink simulation package. The system parameters of the induction motor tested in this study are given in the Appendix.

Electromagnetic torque follows the load torque, and the stator current has a very good dynamic and estimation accuracy, where the real and estimated current shows a perfect superposition. The quadratic rotor flux component Φ_{qr} is maintained to almost zero. Direct rotor flux component Φ_{dr} tracks the reference values adequately well.

The speed reverse test is realized by reverse speed reference (25; -25 rpm) under nominal load torque, which applied at *t*=0.5s, where it is noted that the real rotor speed converges to the reference speed with very less errors and without any significant overshoot. The application of the load does not affect the rotor speed as shown in Figs. 7a and 8. The performance of the controller reveals a good robustness and convergence at rated and low speeds.

5.2 Fault detection and diagnosis of the machine

The fault detection and diagnosis approach of IM in closed loop drives is given in the following steps:

Firstly, on-line fault detection using the model-based technique in order to highlight the appearance of incipient faults based on residual stator current. Finally, off-line diagnosis using a multi-neuro-fuzzy technique based on HFFT analysis of stator current.

5.2.1 IM fault detection

In order to detect faults and study their influences on the residual stator current of IM controlled by feedback linearization, the simulations are carried out with low SNR (10 dB), a reference speed equal to 2600 rpm and a load torque (T_L=3.5 Nm) applied at *t*=0.5s. All faults are realised at *t*=1s and their severities changed at *t*=2s as illustrated in Figs. 9, 10, 11 and 12.

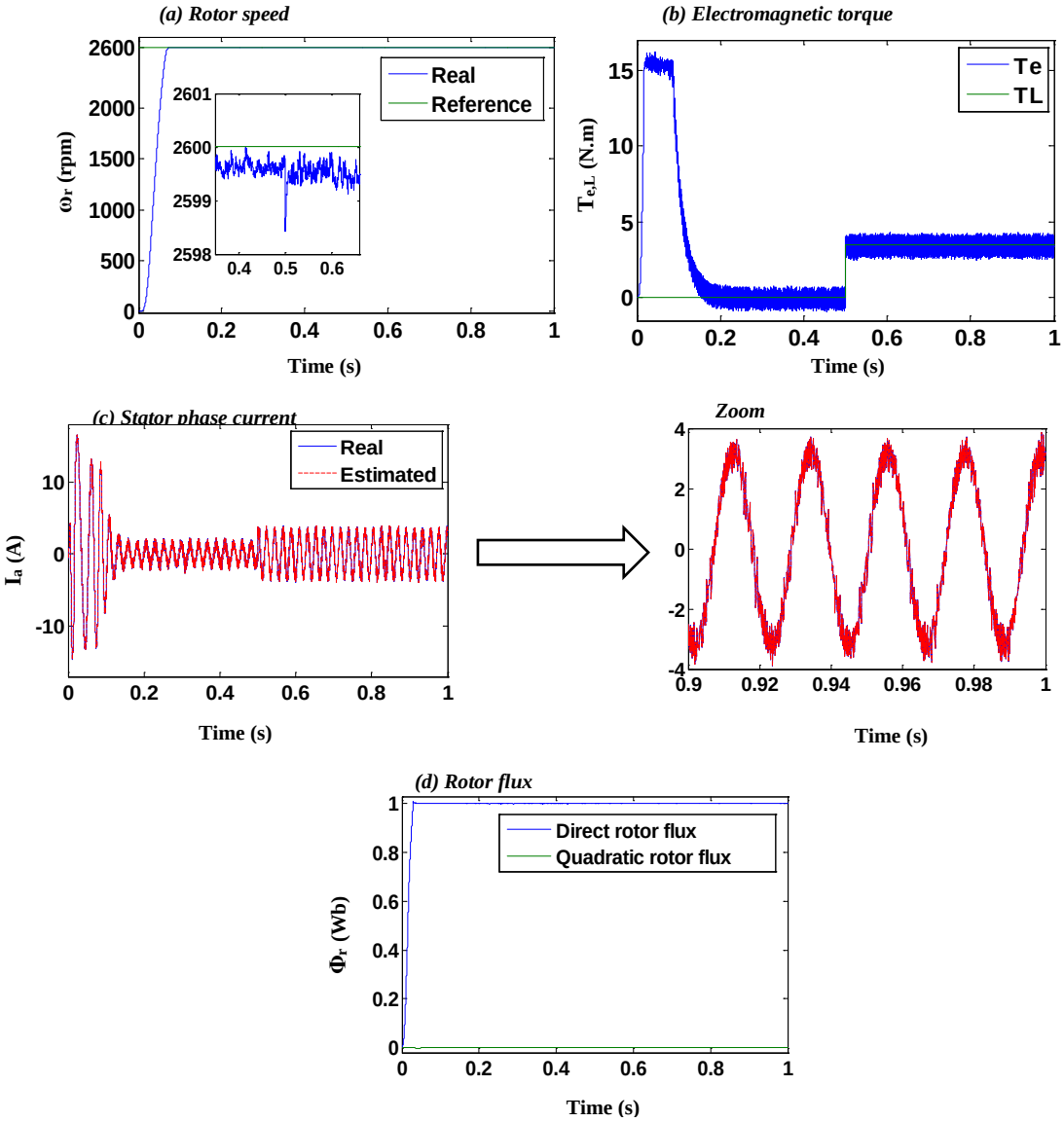

Figure 7. Electric magnetic and mechanical characteristics for input-output feedback linearization control of IM.

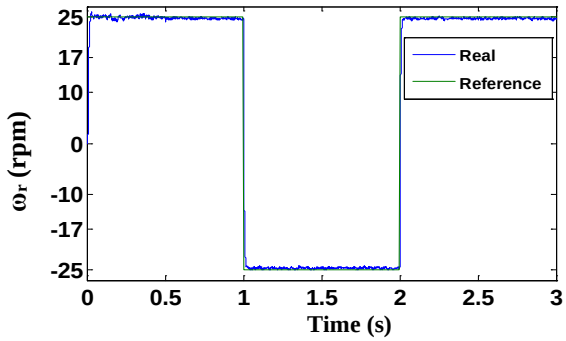

Figure 8. Reverse low speed test.

Figs 9, 10, 11, 12 and Table 1 show that the residual currents start with a very small value in a healthy state, so-called the threshold $\|r_{Ia}\| = 0.1$ A, then increase abruptly when the broken rotor bar, static air-gap eccentricity or mixed fault occur at $t=1s$ according to the fault types and their severities. This technique can be considered as a reliable indicator for rapid incipient faults detection, even at low slip.

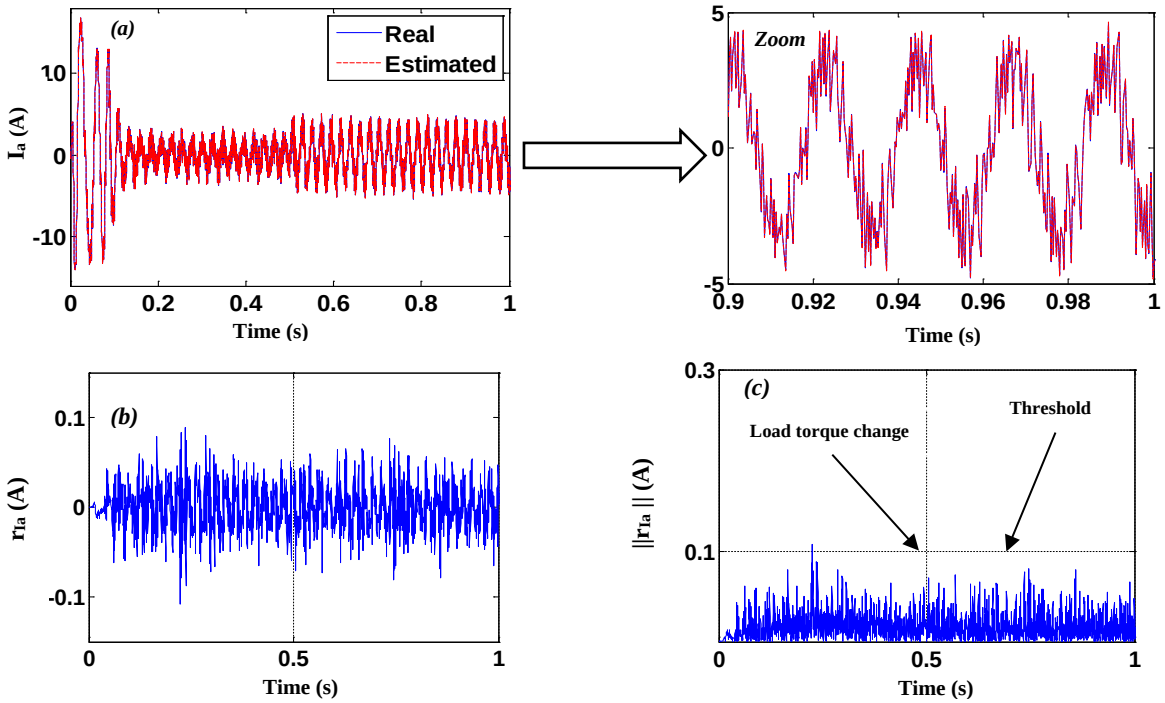

Figure 9. Healthy machine. **a** Stator current with low SNR (10 dB). **b** Stator residual current. **c** Norm of the stator residual current.

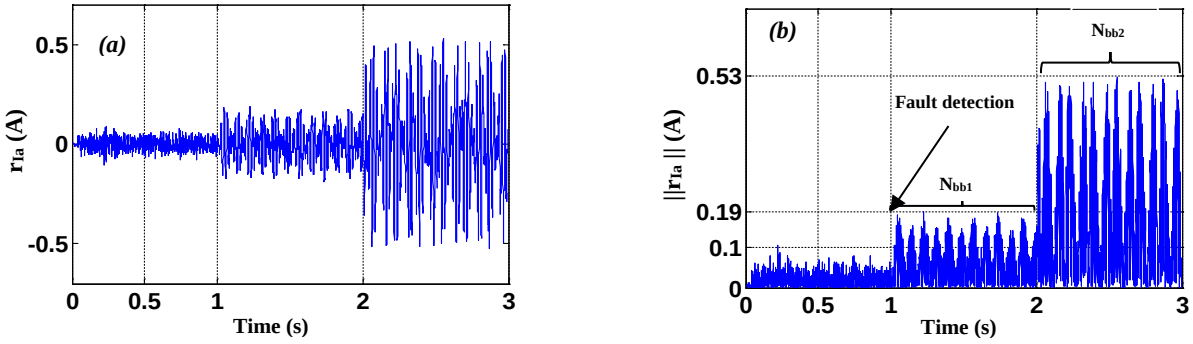

Figure 10. Broken rotor bars fault (N_{bb1}, N_{bb2}). **a** Stator residual current. **b** Norm of the stator residual current.

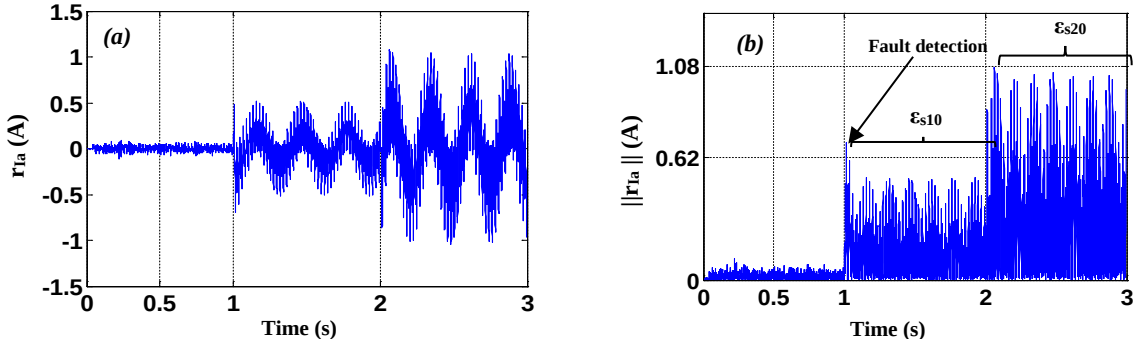

Figure 11. Static air-gap eccentricity (ε_{s10}, ε_{s20}). **a** Stator residual current. **b** Norm of the stator residual current.

However, the $||r_{Ia}||$ are not only very sensitive to the faults occurrence but also to the modelling uncertainties, parameter variation, and unknown inputs such as external noise, which lead to false fault detection. To overcome this problem, neuro-fuzzy technique based on the proprieties of HFFT analysis is applied to confirm the true/false fault detection and identify the faults occurred in the IM.

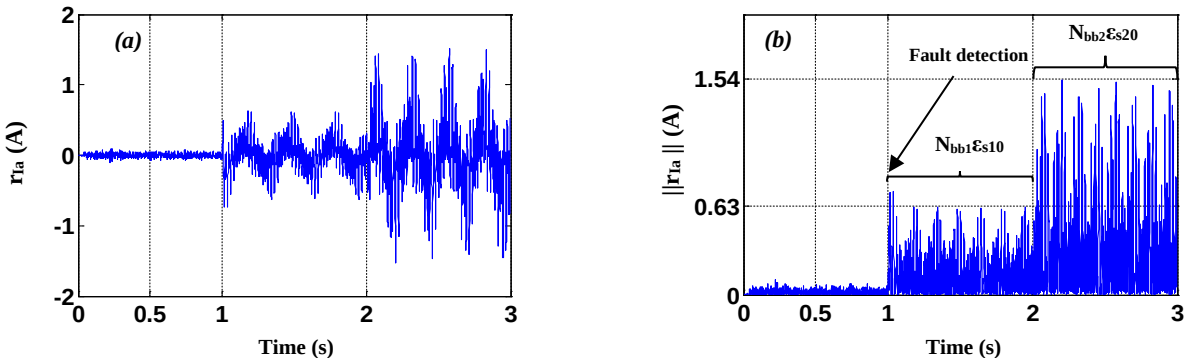

Figure 12. Mixed fault ($N_{bb1}\varepsilon_{s10,}$ $N_{bb2}\varepsilon_{s20}$). **a** Stator residual current. **b** Norm of the stator residual

Table. 1 Severities of $||r_{Ia}||$ for the different defects

Motor states	$\|\|r_{Ia}\|\|$ **(A)**
Healthy motor	0.10
One broken rotor bar (N_{bb1})	0.19
Two broken rotor bar (N_{bb2})	0.53
10% of static air-gap eccentricity (ε_{s10})	0.62
20% of static air-gap eccentricity (ε_{s20})	1.08
Mixed fault ($N_{bb1}\varepsilon_{s10}$)	0.63
Mixed fault ($N_{bb2}\varepsilon_{s20}$)	1.54

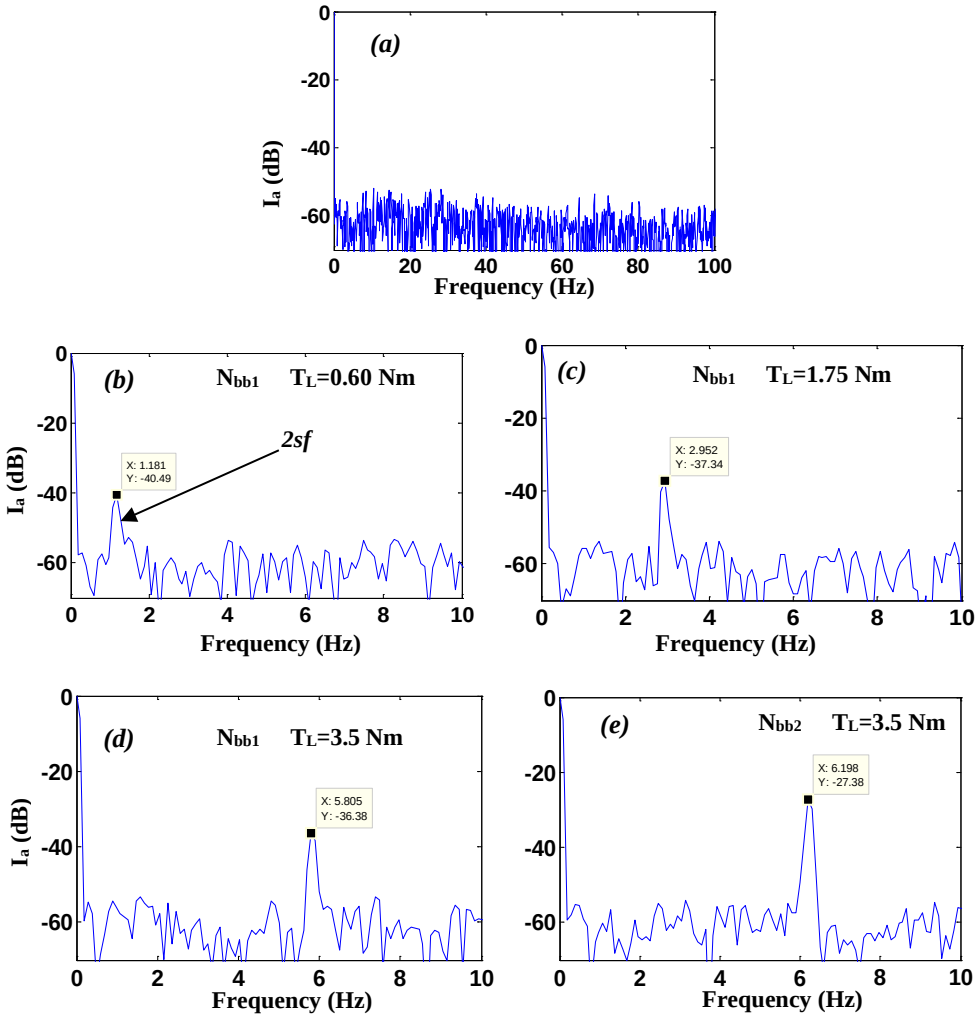

Figure 13. HFFT of the stator current. **a** Healthy motor. **b**, **c**, **d** One broken rotor bar under different loads. **e** Two broken rotor bars.

5.2.2 Extraction of fault indicators

The spectrum analysis is performed on the stator current envelope using HFFT technique in order to extract the fault indicators under different load conditions (full load, half load and low load) and different severities of broken rotor bars and static air-gap eccentricity faults, as shown in Figs. 13 and 14. Mixed fault composite of one broken bar and 10% of static air-gap eccentricity ($N_{bb1\varepsilon_{s10}}$) is illustrated in Fig. 15. The HFFT signatures have been collected at a sampling rate of 10kS/s for the duration of 12s in each case.

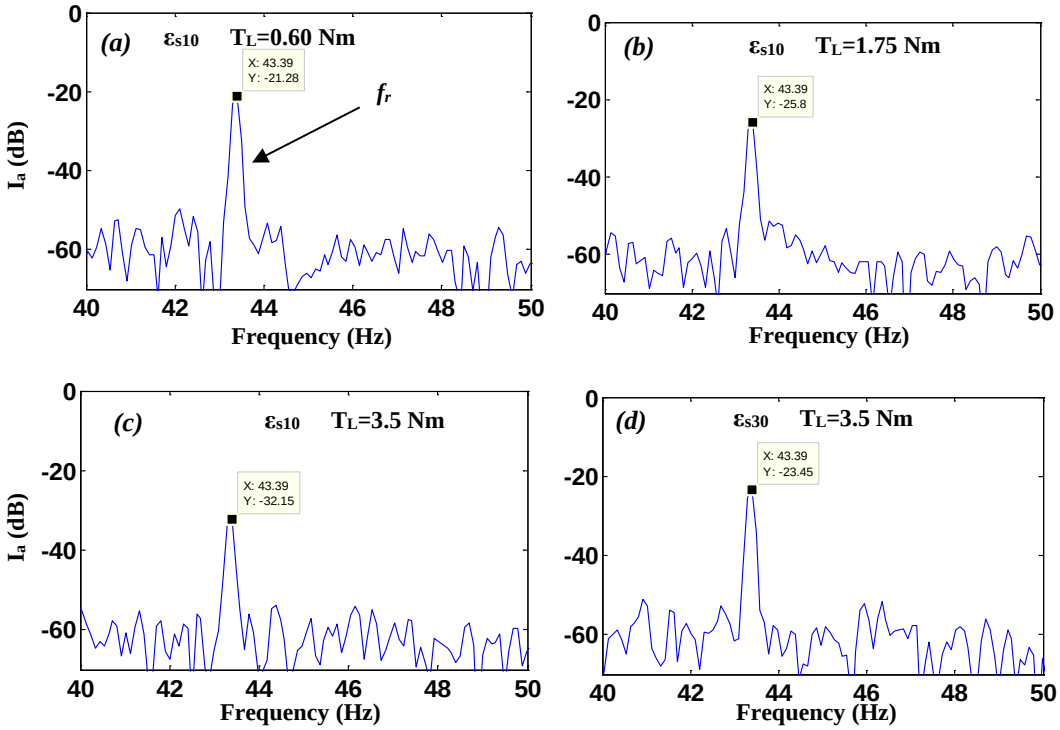

Figure 14. HFFT of the stator current. **a**, **b, c** 10% of static air-gap eccentricity fault under different loads. **d** 30% of static air-gap eccentricity fault.

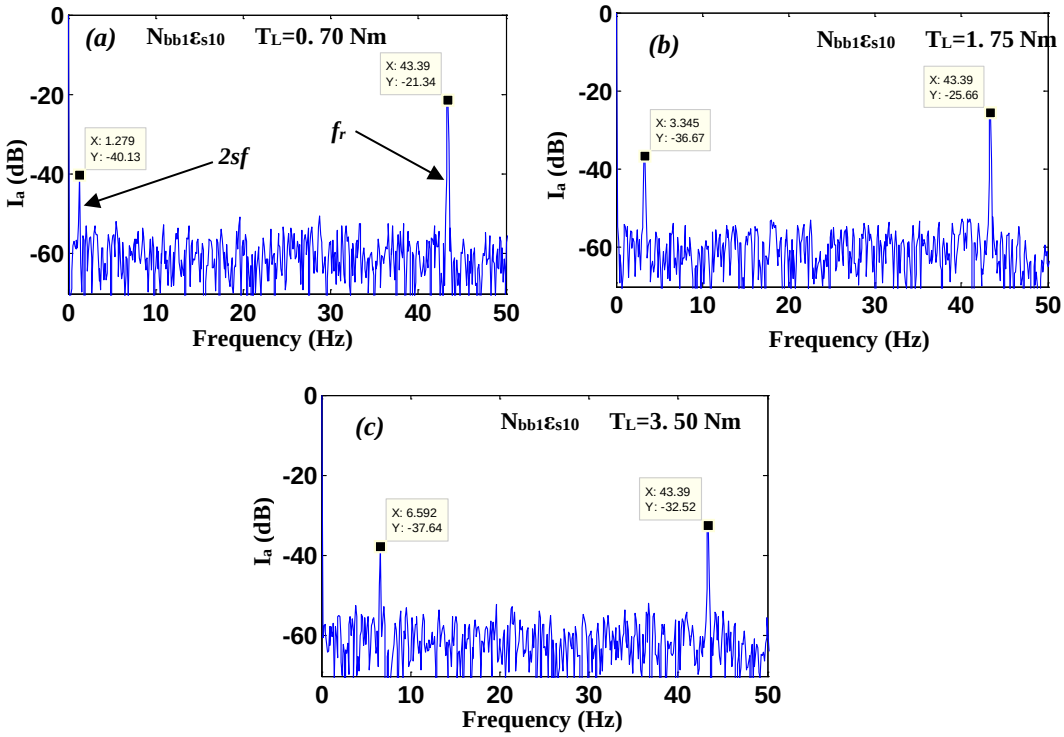

Figure 15. HFFT of the stator current. **a**, **b, c** mixed fault ($N_{bb1\varepsilon_{s10}}$) under different loads.

Figs 13, 14, 15 and Table 2 show the position of the fault harmonics appeared in frequencies *2sf* and f_r, respectively, for broken rotor bars and static air-gap eccentricity. However, the amplitude of the harmonic fault and its position due to broken rotor bars is very sensitive to the load varies, also to the defect severity (number of broken bars). Unlike, the position of the harmonic fault generated by static air-gap eccentricity kept the same position but its amplitude is affected by the defect severity. Therefore, by the surveillance of the amplitudes evaluation of the fault harmonics, the motor state can be predicted by using these relevant indicators.

Table. 2 Magnitude and frequencies of the stator phase current I_a spectrum with different loads and fault severities

Severity	Harmonic (Hz)	Load (Nm)	Slip	$f_{calculated}$ (Hz)	$f_{deduced}$ (Hz)	Magnitude (dB)
N_{bb1}	*2sf*	0.60	0.0134	1.178	1.181	-40.49
N_{bb1}	*2sf*	1.75	0.0325	2.911	2.952	-37.34
N_{bb1}	*2sf*	3.50	0.0627	5.798	5.805	-36.38
N_{bb2}	*2sf*	3.50	0.0667	6.195	6.198	-27.38
ε_{s10}	f_r	0.60	0.0134	43.34	43.39	-21.28
ε_{s10}	f_r	1.75	0.0349	43.34	43.39	-25.80
ε_{s10}	f_r	3.50	0.0696	43.34	43.39	-32.15
ε_{s30}	f_r	3.50	0.0704	43.34	43.39	-23.45
$N_{bb1}\varepsilon_{s10}$	*2sf*, f_r	0.60	0.0145	2.275, 43.34	1.279, 43.39	-40.13, -21.34
$N_{bb1}\varepsilon_{s10}$	*2sf*, f_r	1.75	0.0370	3.327, 43.34	3.345,43.39	-36.67, -25.66
$N_{bb1}\varepsilon_{s10}$	*2sf*, f_r	3.50	0.0710	6.622, 43.34	6.592, 43.39	-37.64, -32.52

5.2.3 IM Multi-ANFIS (MANFIS) diagnosis

A hybrid neuro-fuzzy technique brings the learning capabilities of neural networks to the fuzzy inference system of the Takagi-Sugeno type. The role of learning is the adjustment of the parameters of this fuzzy inference system. The strength of the adaptive neuro-fuzzy inference system is the ability to generate fuzzy rules using subtractive clustering or grid partitioning [49]. However, ANFIS is only suitable for the single output system. For a system with multiple outputs, ANFIS is placed side by side to produce a MANFIS. The number of ANFIS depends on the number of outputs required, and the input data is coupled to the separate outputs. Fig. 16 shows MANFIS architecture, the input data remains the same for each ANFIS; they also have the same initial parameters such as the initial step size, membership function type and number.

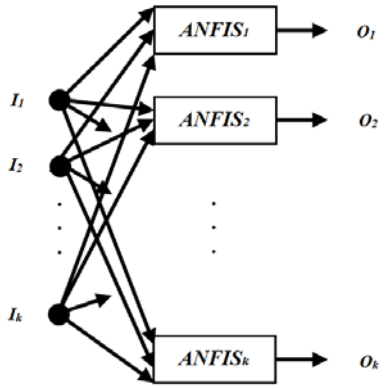

Figure 16. MENFIS architecture.

MANFIS network is used to identify automatically the broken rotor bars, static air-gap eccentricity faults, or both faults at the same time.

Two of the fault indicators have been chosen and grouped in a vector $I_i = [I_1; I_2]$ presents the input vector data of the MANFIS network as illustrated in Fig. 17. Where I_1 and I_2 are respectively, the amplitude of harmonics *2sf* and f_r which are extracted from the simulation of the current envelope spectrum under different loads and fault severities.

The MANFIS network is setting into two outputs, grouped in a vector $O_i = [O_1; O_2]$ indicates the broken rotor bars and static air-gap eccentricity faults, respectively. These Outputs are constructed by matching each sample in the input data set by its desired output T_i. The targets obtained $T_i = [T_1; T_2]$ are coded in binary, as follows:

T_i = [0; 0]: healthy motor,

T_i = [1; 0]: broken rotor bars fault,

T_i = [0; 1]: static air-gap eccentricity fault,

T_i = [1; 1]: mixed fault.

The input vector data I_i is constituted by a successive series of samples, characterizing the operation of the healthy and faulty machine under five different loads (T_L= 0.35, 1.05, 1.75, 2.45, 3.5 Nm) as follows:

1) Healthy motor (5 samples),

2) Broken rotor bars fault: N_{bb1} and N_{bb2} (5+5=10 samples),

3) Static air-gap eccentricity fault: ε_{s10} and ε_{s30} (5+5=10 samples),

4) Mixed fault (broken rotor bars and static air-gap eccentricity): $N_{bb1}\varepsilon_{s10}$, $N_{bb1}\varepsilon_{s30}$, $N_{bb2}\varepsilon_{s10}$, and $N_{bb2}\varepsilon_{s30}$ (5+5+5+5=20 samples).

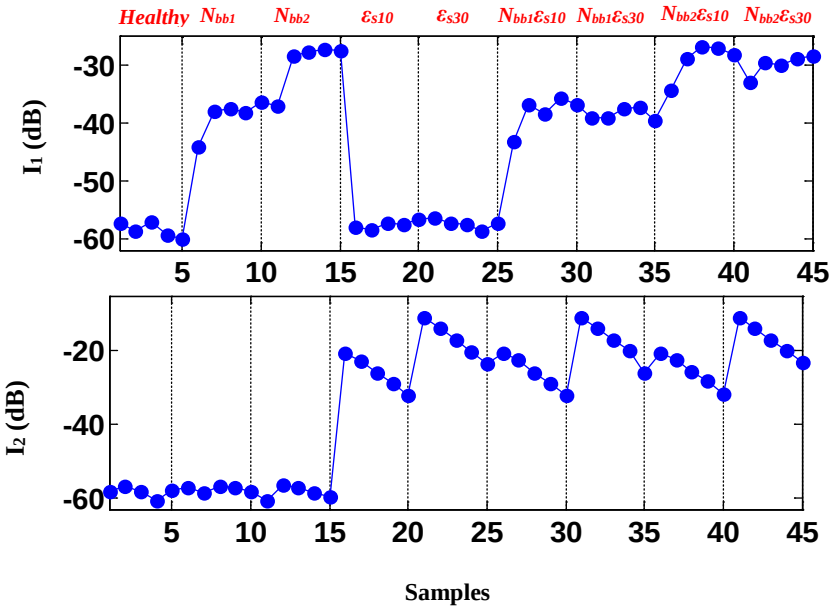

Figure 17. Training input data set of MANFIS.

The network designed MANFIS consists of two ANFIS, each ANFIS has two inputs and one output. The input variables are I_1 and I_2, and the output variables are O_1 for ANFIS$_1$ and O_2 for ANFIS$_2$. For each input variable, three Gaussian membership functions are used.

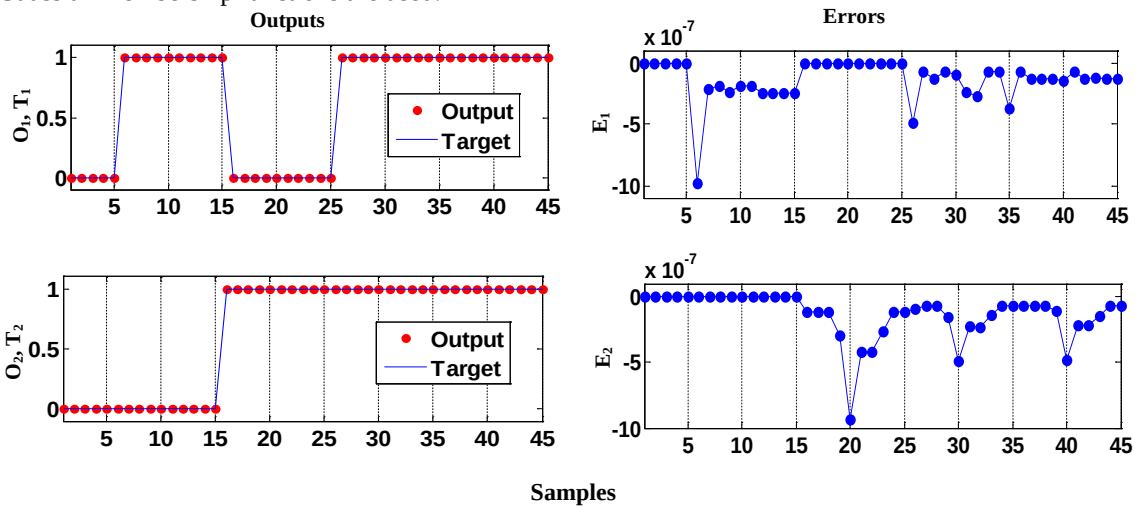

Figure 18. Training and errors outputs of MANFIS.

The outputs data, as well as network learning errors, are shown in Fig. 18. We noticed that the learning errors are very less, which proves that the network has learned well sequences of broken rotor bars and air-gap eccentricity failures.

The MANFIS diagnosis system has been tested under different loads and fault severities not taken in the learning phase of the machine (T_L=0.7, 2.1, 2.8 Nm).

For a simple fault (Fig. 19):

1) Healthy motor (3 samples),

2) Broken rotor bars fault: N_{bb1} and N_{bb2} (3+3=6 samples),

3) Static air-gap eccentricity fault: ε_{s20} and ε_{s40} (3+3=6 samples).

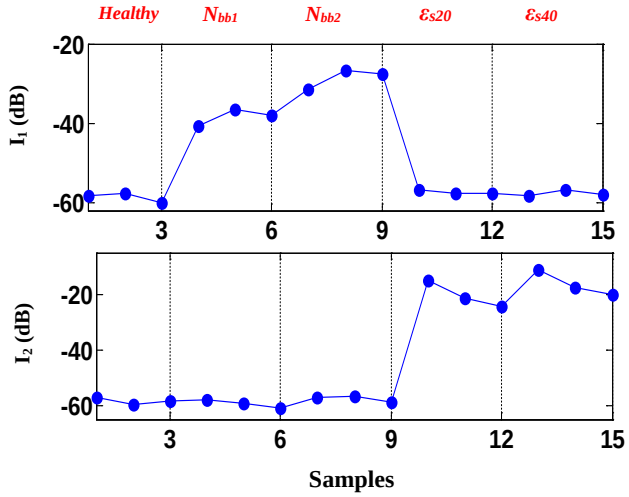

Figure 19. Input data set of MANFIS test for a simple fault

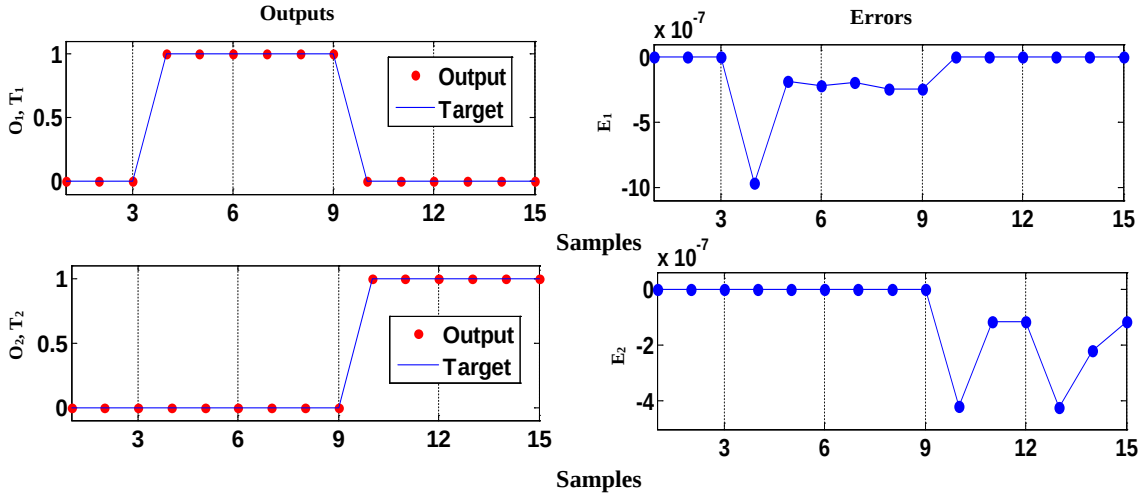

Figure 20. MANFIS test and outputs errors for a simple fault.

For a mixed fault (Fig. 21):

1) Healthy motor (3 samples),

2) Mixed fault (broken rotor bars and static air-gap eccentricity): $N_{bb1}\varepsilon_{s20}$ and $N_{bb2}\varepsilon_{s40}$ (3+3=6 samples).

The results of the test illustrated in Figs. 20 and 22 show that the MANFIS outputs and their errors are able to report automatically in an efficient and reliable way the simple and mixed broken rotor bars and static air-gap eccentricity defects from the beginning of their appearances. This system also has a high accuracy to correctly distinguish between the healthy and faulty machine under different severities and load conditions.

Table 3 presents a summary of other works and their respective results for comparison purposes.

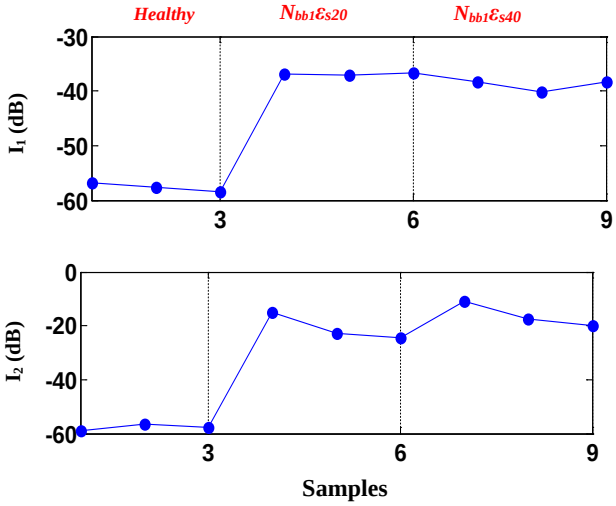

Fig. 21. Input data set of MANFIS test for a mixed fault

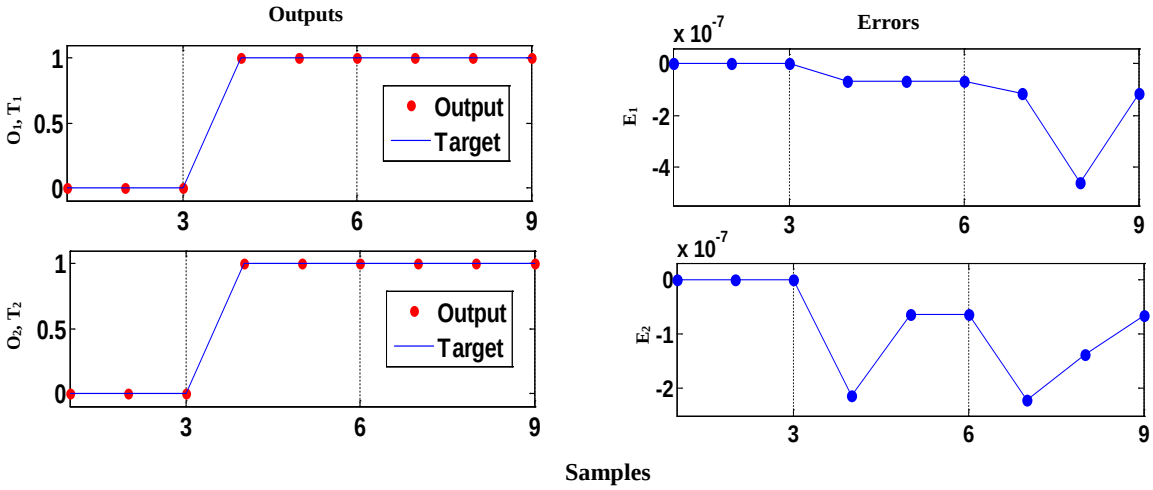

Figure 22. MANFIS test and outputs errors for a mixed fault.

6. Conclusion

This paper presents a fast detection and recognition approach of the mixed and simple fault, particularly, the broken rotor bars and the static air-gap eccentricity faults for IM in the closed-loop drive. The IOFL control is introduced in order to ensure the operation continuity of defected IM and to investigate the fault effect. A reduced model of IM with a rotor cage has been implemented in order to simulate the proposed faults, and also for the control and observer design.

This advanced approach required a good knowledge of the system, which leads to adopting two strategies for detection and diagnosis of the defects. Foremost, model-based strategy with the contribution of SMO has been used to generate the residual stator current for rapid incipient fault detection in the control scheme. Furthermore, the MANFIS technique is used to confirm if the residuals detected are induced by the faults or other disturbances, also distinguish and identify these faults. However, the amplitudes of fault harmonics 2sf and fr, respectively, due to the broken rotor bars and static air-gap eccentricity, are obtained via HFFT analysis under different load conditions and fault severities. These relevant amplitudes have been used as fault indicators and have been considered as two inputs data for the MANFIS. Moreover, the two MANFIS outputs data provide a high accuracy on the information of two defects studied, and prove that it is able to identify the fault types in the machines. The results obtained with this proposed approach are efficient and accurate to detect and identify the rotor faults of the IM operating in the closed-loop drive.

Table. 3 Summary of the recently published papers in comparison with the present research

Reference	Fault type (simple / mixed)	Low load	Motor control drive	Observer	Online fault detection	Magnitudes, Signal processing	Artificial intelligence technique	Accuracy fault identification
[31]	Broken rotor bars (simple)	Yes	Open loop	No	No	Magnetic flux, FFT	ANFIS	99%
[32]	stator winding (simple)	Not reported	Open loop	No	No	Stator current, SCAI and SCPI	ANFIS	Not reported
[35]	Broken rotor bars, stator winding and unbalanced supply (simple)	Not reported	Open loop	No	PSD	Stator current, PSD and FFT	FMM-CART	100%
[36]	Broken rotor bars (simple)	No	Open loop	No	No	Stator current, FFT	ORF	81.5%
[38]	Bearing (simple)	Not reported	Open loop	No	No	vibration signal, SK	KNN	Not reported
[37]	bearing (simple)	Not reported	Open loop	No	No	acoustic emission signal, LDA	NB	99.44%
[40]	Broken rotor bars (simple)	Not reported	Open loop	No	No	Stator current, SWPT	SVDD	100%
[41]	stator winding (simple)	Yes	Open loop	No	No	Stator current, phase shift	NN	100%
[39]	bearing (simple)	No	Open loop	No	No	vibration signal, CSM	ADCNN	95.75%
This research	Broken rotor bars and static eccentricity (simple/ mixed)	Yes	IOFL	SMO	Residual generation	Stator current, HFFT	MANFIS	100%

Nomenclature

U_{ds}, U_{qs}	*(d,q)* axis voltages of the stator	μ_0	Magnetic permeability of the air
I_{ds}, I_{qs}	*(d,q)* axis current components of the stator	p	Number of pole pairs
I_{dr}, I_{qr}	*(d,q)* axis current components of the rotor	e	Air-gap mean diameter
I_e	Short circuit ring current	α	Angle between two broken rotor bars
$[U]$	Voltage vector	R_s	Stator resistance
$[I]$	Current vector	R_r	Rotor resistance
$[L]$	Inductance matrix	R_b	Rotor bar resistance
$[R]$	Resistance matrix	R_e	Resistance of end ring segment
R	Average radius of the air gap	L_b	Rotor bar inductance
U_{dc}	Direct voltage	L_e	Inductance of end ring
U_a, U_b, U_c	Three phases voltages a, b, c	L_{sf}	Leakage inductance of stator
I_a, I_b, I_c	Three phases current a, b, c of the stator	M_{sr}	Mutual inductance
$U_{s\alpha}$, $U_{s\beta}$	*(α,β)* axis voltages of the stator	N_s	Number of turns per stator phase
ω_r	electrical rotor speed in rpm	N_r	Number of rotor bars
ω_{ref}, Φ_{ref}	Rotor reference speed and flux	L	Length of the rotor
N_{bbk}	Number of broken rotor bars	J	Inertia moment
Y	measurable output	F	Coefficient of damping
U	control variable	T_e , T_L	Electromagnetic torque, load torque

X	State variable	i_{bk}	Current of the bar k
i_{rk}	Current of the loop k	i_{ek}	Short circuit ring current of the portion k
$\varepsilon_{sk\%}$	Static air-gap eccentricity of $k\%$ degree	φ	Particular position along the stator inner surface
θ_r	Angular position of the rotor with respect to some stator reference	g_e^{-1}	Inverse gap function
l	Length of the rotor	s	Rotor slip
f	Stator frequency	f_r	Rotor frequency
FMM-CART	Fuzzy Min-Max- Classification and Regression Tree	***ORF***	Oblique Random Forest
KNN	K-Nearest Neighbor	***NB***	Naive Bayes
SVDD	Support Vector Data Description	***NN***	Neural Networks
ADCNN	Adaptive Deep Convolutional Neural Network	***SCAI***	Sequence Component Amplitude Index
SCPI	Component Phase Index	***PSD***	Power Spectral Density
SK	Spectral Kurtosis	***LDA***	Linear Discriminant Analysis
SWPT	Stationary Wavelet Packet Transform	***CSM***	Cyclic Spectrum Maps

Appendix

Parameters for the simulation of the IM

P_n	Output power	1.1kW
U_s	Stator voltage	220 V
f	Stator frequency	50 Hz
p	Number of pole pairs	1
R_s	Stator resistance	7.58 Ω
R_r	Rotor resistance	6.3 Ω
R_b	Rotor bar resistance	0.15 m Ω
R_e	Resistance of end ring segment	0.15 m Ω
L_b	Rotor bar inductance	0.1 µH
L_e	Inductance of end ring	0.1 µH
L_{sf}	Leakage inductance of stator	26.5 mH
M_{sr}	Mutual inductance	46.42 mH
N_s	Number of turns per stator phase	160
N_r	Number of rotor bars	16
l	Length of the rotor	65 mm
e	Air-gap mean diameter	2.5mm
J	Inertia moment	0.0054 kgm2
F	Coefficient of damping	0.0029 Nm/rad/s
T_e , T_L	Electromagnetic torque, load torque	

7. References

[1] Abd-el-Malek MB, Abdelsalam AK, Hassan OE. Novel approach using Hilbert Transform for multiple broken rotor bars fault location detection for three phase induction motor. ISA Trans. 2018;80:439–457.

[2] Ameid T, Menacer A, Talhaoui H, Azzoug Y. Discrete wavelet transform and energy eigen value for rotor bars fault detection in variable speed field-oriented control of induction motor drive. ISA Trans. 2018;79:217–231.

[3] Ammar A, Bourek A, Benakcha A. Nonlinear SVM-DTC for induction motor drive using input-output feedback linearization and high order sliding mode control. ISA Trans. 2017;67:428–442.

[4] Sarkar SK, Das SK. High performance nonlinear controller design for AC and DC machines: partial feedback linearization approach. Int J Dyn Control. 2018;6:679–693.

[5] Mishra RN, Mohanty KB. Implementation of feedback-linearization-modelled induction motor drive through an adaptive simplified neuro-fuzzy approach. Sādhanā. 2017;42:2113–2135.

[6] Guven Y, Atis S. Implementation of an embedded system for real-time detection of rotor bar failures in induction motors. ISA Trans. 2018;81:210–221.

[7] Jafarian MJ, Nazarzadeh J. Employing neutral-voltage spectrum for internal turn-to-turn fault detection in the induction machine drives. ISA Trans. 2018;81:306–317.

[8] Li DZ, Wang W, Ismail F. An intelligent harmonic synthesis technique for air-gap eccentricity fault diagnosis in induction motors. Chinese J Mech Eng. 2017;30:1296–1304.
[9] Menacer A, Moreau S, Benakcha A, Nait Said M. Effect of the Position and the Number of Broken Bars on Asynchronous Motor Stator Current Spectrum. 2006 12th Int. Power Electron. Motion Control Conf., IEEE; 2006, p. 973–978.
[10] Duvvuri S, Detroja K. Model-based broken rotor bars fault detection and diagnosis in squirrel-cage induction motors. 2016 3rd Conf. Control Fault-Tolerant Syst., IEEE; 2016, p. 537–539.
[11] Chang H-C, Lin S-C, Kuo C-C, Hsieh C-F. Induction Motor Diagnostic System Based on Electrical Detection Method and Fuzzy Algorithm. Int J Fuzzy Syst. 2016;18:732–740.
[12] Xiong H, Liao Y, Chu X, Nian X, Wang H. Observer based fault tolerant control for a class of Two-PMSMs systems. ISA Trans. 2018;80:99–110.
[13] Mapelli FL, Tarsitano D, Cheli F. MRAS rotor resistance estimators for EV vector controlled induction motor traction drive: Analysis and experimental results. Electr Power Syst Res. 2017;146:298–307.
[14] Echeikh H, Trabelsi R, Iqbal A, Mimouni MF. Real time implementation of indirect rotor flux oriented control of a five-phase induction motor with novel rotor resistance adaption using sliding mode observer. J Franklin Inst. 2018;355:2112–2141.
[15] Ammar A, Bourek A, Benakcha A. Sensorless SVM-Direct Torque Control for Induction Motor Drive Using Sliding Mode Observers. J Control Autom Electr Syst. 2017;28:189–202.
[16] Talhaoui H, Menacer A, Kessal A, Kechida R. Fast Fourier and discrete wavelet transforms applied to sensorless vector control induction motor for rotor bar faults diagnosis. ISA Trans. 2014;53:1639–1649.
[17] Maouche A, M'Saad M, Bensaker B, Farza M. High gain adaptive observer design for sensorless state and parameter estimation of induction motors. Int J Control Autom Syst. 2015;13:1106–1117.
[18] Dyskin A V., Basarir H, Doherty J, Elchalakani M, Joldes GR, Karrech A, et al. Computational monitoring in real time: review of methods and applications. Geomech Geophys Geo-Energy Geo-Resources. 2018;4:235–271.
[19] Dybkowski M, Klimkowski K. Speed sensor fault detection algorithm for vector control methods based on the parity relations. 2017 19th Eur. Conf. Power Electron. Appl. (EPE'17 ECCE Eur)., IEEE; 2017, p. P.1-5.
[20] De Angelo CH, Bossio GR, Giaccone SJ, Valla MI, Solsona JA, Garcia GO. Online Model-Based Stator-Fault Detection and Identification in Induction Motors. IEEE Trans Ind Electron. 2009;56:4671–4680.
[21] Guezmil A, Berriri H, Pusca R, Sakly A, Romary R, Mimouni MF. Detecting Inter-Turn Short-Circuit Fault in Induction Machine Using High-Order Sliding Mode Observer: Simulation and Experimental Verification. J Control Autom Electr Syst. 2017;28:532–540.
[22] Duvvuri SSSRS, Detroja K. Model-based stator interturn short-circuit fault detection and diagnosis in induction motors. 2015 7th Int. Conf. Inf. Technol. Electr. Eng., IEEE; 2015, p. 167–172.
[23] Bárcenas E, Lugo-Cordero LF, Campos-Delgado DU, Hernández-Díez JE, Espinoza-Trejo DR, Bossio G. Fault diagnosis scheme for open-circuit faults in field-oriented control induction motor drives. IET Power Electron. 2013;6:869–877.
[24] Verrelli CM, Lorenzani E, Fornari R, Mengoni M, Zarri L. Steady-state speed sensor fault detection in induction motors with uncertain parameters: A matter of algebraic equations. Control Eng Pract. 2018;80:125–137.
[25] Talhaoui H, Menacer A, Kessal A, Tarek A. Experimental diagnosis of broken rotor bars fault in induction machine based on Hilbert and discrete wavelet transforms. Int J Adv Manuf Technol 2018;95:1399–1408.
[26] Saidi L, Fnaiech F, Henao H, Capolino G-A, Cirrincione G. Diagnosis of broken-bars fault in induction machines using higher order spectral analysis. ISA Trans 2013;52:140–148.
[27] Abd-el-Malek MB, Abdelsalam AK, Hassan OE. Novel approach using Hilbert Transform for multiple broken rotor bars fault location detection for three phase induction motor. ISA Trans 2018;80:439–457.
[28] Liu R, Yang B, Zio E, Chen X. Artificial intelligence for fault diagnosis of rotating machinery: A review. Mech Syst Signal Process 2018;108:33–47.
[29] Gao XZ, Wang X, Zenger K. Motor fault diagnosis using negative selection algorithm. Neural Comput Appl 2014;25:55–65.
[30] Goode PV, Mo-Yuen Chow. Using a neural/fuzzy system to extract heuristic knowledge of incipient faults in induction motors: Part II-Application. IEEE Trans Ind Electron 1995;42:139–146.
[31] Dias CG, de Sousa CM. A Neuro-Fuzzy Approach for Locating Broken Rotor Bars in Induction Motors at Very Low Slip. J Control Autom Electr Syst 2018;29:489–499.
[32] Samanta S, Bera JN, Sarkar G. Severity and Location Detection of Three Phase Induction Motor Stator Fault Using Sample Shifting Technique and Adaptive Neuro Fuzzy Inference System. In: Chattopadhyay S, Roy T, Sengupta S, Berger-Vachon C, editors. Modelling and Simulation in Science, Technology and Engineering Mathematics, vol. 749, Cham: Springer International Publishing; 2019, p. 423–437.

[33] Karnavas YL, Chasiotis ID, Vrangas A. Fault diagnosis of squirrel-cage induction motor broken bars based on a model identification method with subtractive clustering. 2017 IEEE 11th Int. Symp. Diagnostics Electr. Mach. Power Electron. Drives, vol. 2017–Janua, IEEE; 2017, p. 304–310.
[34] Souad L, Azzedine B, Eddine CBD, Boualem B, Samir M, Youcef M. Induction machine rotor and stator faults detection by applying the DTW and N-F network. 2018 IEEE Int. Conf. Ind. Technol., IEEE; 2018, p. 431–436.
[35] Seera M, Lim CP, Ishak D, Singh H. Offline and online fault detection and diagnosis of induction motors using a hybrid soft computing model. Appl Soft Comput 2013;13:4493–4507.
[36] Martin-Diaz I, Morinigo-Sotelo D, Duque-Perez O, Osornio-Rios RA, Romero-Troncoso RJ. Hybrid algorithmic approach oriented to incipient rotor fault diagnosis on induction motors. ISA Trans 2018;80:427–438.
[37] Nguyen PH, Kim J-M. Multifault Diagnosis of Rolling Element Bearings Using a Wavelet Kurtogram and Vector Median-Based Feature Analysis. Shock Vib 2015;2015:1–14.
[38] Tian J, Morillo C, Azarian MH, Pecht M. Motor Bearing Fault Detection Using Spectral Kurtosis-Based Feature Extraction Coupled With K-Nearest Neighbor Distance Analysis. IEEE Trans Ind Electron 2016;63:1793–1803.
[39] Islam MMM, Kim J-M. Motor Bearing Fault Diagnosis Using Deep Convolutional Neural Networks with 2D Analysis of Vibration Signal. Adv. Artif. Intell., Springer International Publishing; 2018, p. 144–155.
[40] Zgarni S, Keskes H, Braham A. Nested SVDD in DAG SVM for induction motor condition monitoring. Eng Appl Artif Intell 2018;71:210–215.
[41] Bensaoucha S, Ameur A, Bessedik SA, Moati Y. Artificial Neural Networks Technique to Detect and Locate an Interturn Short-Circuit Fault in Induction Motor. In: Hatti M, editor. Renewable Energy for Smart and Sustainable Cities, vol. 62, Cham: Springer International Publishing; 2019, p. 103–113.
[42] Ertunc HM, Ocak H, Aliustaoglu C. ANN- and ANFIS-based multi-staged decision algorithm for the detection and diagnosis of bearing faults. Neural Comput Appl 2013;22:435–446.
[43] Ameid T, Menacer A, Talhaoui H, Harzelli I. Broken rotor bar fault diagnosis using fast Fourier transform applied to field-oriented control induction machine: simulation and experimental study. Int J Adv Manuf Technol 2017;92:917–928.
[44] Rangel-Magdaleno J, Peregrina-Barreto H, Ramirez-Cortes J, Cruz-Vega I. Hilbert spectrum analysis of induction motors for the detection of incipient broken rotor bars. Measurement 2017;109:247–255.
[45] Ameid T, Menacer A, Talhaoui H, Harzelli I. Rotor resistance estimation using Extended Kalman filter and spectral analysis for rotor bar fault diagnosis of sensorless vector control induction motor. Measurement 2017;111:243–259.
[46] Harzelli I, Menacer A, Ameid T. A fault monitoring approach using model-based and neural network techniques applied to input–output feedback linearization control induction motor. J Ambient Intell Humaniz Comput 2019;11:2519-2538.
[47] Kaikaa MY, Hadjami M, Khezzar A. Effects of the simultaneous presence of static eccentricity and broken rotor bars on the stator current of induction machine. IEEE Trans Ind Electron 2014;61:2452–2463.
[48] Oumaamar MEK, Maouche Y, Boucherma M, Khezzar A. Static air-gap eccentricity fault diagnosis using rotor slot harmonics in line neutral voltage of three-phase squirrel cage induction motor. Mech Syst Signal Process 2017;84:584–597.
[49] Jang J-SR. ANFIS: adaptive-network-based fuzzy inference system. IEEE Trans Syst Man Cybern 1993;23:665–685.